Key Points:
- First time such a large number (13) of space-ground conjugated events of magnetospheric whistler-mode ELF/VLF waves is reported
- Ionospheric exit point of the waves is usually located at least ~250 km equatorwards (south) of ground station in Finland at L ~5.5
- All conjugated events but one were observed on the afternoon side of the magnetosphere

Multievent Study of Characteristics and Propagation of Naturally Occurring ELF/VLF Waves Using High-Latitude Ground Observations and Conjunctions With the Arase Satellite

C. Martinez-Calderon[1,2] , Y. Katoh[1] , J. Manninen[3] , O. Santolik[4,5] , Y. Kasahara[6] , S. Matsuda[7] , A. Kumamoto[1] , F. Tsuchiya[1] , A. Matsuoka[7] , M. Shoji[2] , M. Teramoto[8] , I. Shinohara[7] , K. Shiokawa[2] , and Y. Miyoshi[2]

[1]Department of Geophysics, Graduate School of Science, Tohoku University, Sendai, Japan, [2]Institute for Space-Earth Environmental Research, Nagoya University, Nagoya, Japan, [3]Sodankyla Geophysical Observatory, University of Oulu, Sodankyla, Finland, [4]Faculty of Mathematics and Physics, Charles University, Prague, Czech Republic, [5]Department of Space Physics, Institute of Atmospheric Physics of the Czech Academy of Sciences, Prague, Czech Republic, [6]Division of Electrical Engineering and Computer Science, Graduate School of Natural Science and Technology, Kanazawa University, Kanazawa, Japan, [7]Institute of Space and Astronautical Science, JAXA, Japan, [8]Department of Space Systems Engineering, Kyushu Institute of Technology, Kitakyushu, Japan

Abstract We report the properties of the ionospheric exit point and characteristics of several types of very low frequency waves, including chorus and quasiperiodic emissions, based on a comprehensive dataset of simultaneous observations between ground and space. Whistler-mode waves were observed at Kannuslehto (L = 5.5, KAN), Finland, and in the inner magnetosphere by the Japanese Arase satellite. During the 2017–2018 winter campaign, we found 13 cases showing one-to-one correspondence of wave spectra between KAN and Arase. This is the first time that such a large number of conjugated events have been reported at once. The duration of the events ranged from a few minutes up to 3 h, with 90% of events detected in the afternoon sector. While the occurrence rate is higher during daytime, this can also be related to a majority of the detected waves being quasiperiodic emissions, a known dayside phenomenon. Arase was usually located within 30° of the equator, at L ~4–5, and detected mostly waves propagating at oblique angles (≥20°). Frequently, the ionospheric magnetic footprint of Arase was located equatorwards (south) from KAN, often in the same geographical area. We investigated the probable location of the ionospheric exit point of the waves from the location of the footprint of Arase and the angle of arrival of waves detected at KAN. Using density measurements at Arase we discuss magnetospheric wave propagation; we find that, in most cases, waves were unducted in their propagation from the satellite to the ground.

1. Introduction

Extremely low frequency (ELF) and very low frequency (VLF) emissions are whistler-mode waves naturally present in the magnetosphere. ELF waves are those observed in the 0.3–3 kHz frequency range and VLF in the 3–30 kHz range (Barr et al., 2000). They are usually generated near the geomagnetic equator through resonant cyclotron interaction with energetic electrons with energies up to several tens of keV (Kennel & Petschek, 1966). ELF/VLF whistler-mode waves propagate at frequencies below the electron cyclotron frequency, typically below 10–12 kHz for the inner magnetosphere (L < 4–5). We usually catalog ELF/VLF emissions according to on their spectral features. Chorus emissions show discrete features consisting of a series of rising or falling frequency tones usually separated by tens of seconds (see reviews by Sazhin and Hayakawa (1992) and Santolik (2008)). Hiss presents as a noise-like broadband emission (Meredith et al., 2007; Thorne et al., 1973), while quasiperiodic emissions (QP) show periodic time modulation of their wave intensity in the order of tens of seconds to several minutes (Sazhin & Hayakawa, 1994; Smith et al., 1998). Bursty-patches are high frequency short bursts lasting less than a few minutes (Martinez-Calderon et al., 2015a; Shiokawa et al., 2014). During their propagation in the magnetosphere, ELF/VLF waves influence electrons with energies from a few keV up to 1 MeV through wave-particle interactions. In some cases, these electrons are accelerated to higher energies (Bortnik & Thorne, 2007; Horne et al., 2005;

Meredith et al., 2003; Miyoshi et al., 2003) while in other cases, the changes in their pitch angle distribution result in electron scattering into the atmosphere (Bortnik & Thorne, 2007; Hayosh et al., 2013; Lyons et al., 1972; Thorne, 2010).

ELF/VLF waves propagate over long distances in the magnetosphere, and under some conditions, penetrate to the ionosphere, sometimes escaping through an ionospheric exit point to the ground where VLF receivers detect them. As whistler-mode propagation time across the magnetosphere is only a few seconds, magnetospheric conditions related to their generation do not change during propagation. The waves carry important information on the plasma parameters of their source region and generation conditions (Demekhov et al., 2017; Kurth et al., 2015; Li et al., 2011; Martinez-Calderon et al., 2019, 2020)

Conjugated observations where we observe waves with the same spectral features on the ground and satellites give us important clues on the properties of waves and the characteristics at the source. Titova et al. (2015) used simultaneous observations of QP emissions between the ground station of Kannuslehto (KAN), Finland, and Van Allen Probe A (RBSP-A) to find the probable location of their source region. Martinez-Calderon et al. (2016) used conjugated observations between a ground station in Athabasca, Canada, and RBSP-B to discuss the propagation path followed by the waves. Using the density profile from the spacecraft, they found that plasma density plays a major role in wave propagation in the magnetosphere. Using RBSP-A and KAN, Demekhov et al. (2017) discussed chorus propagation and preservation of spectral shape during magnetospheric reflection. Martinez-Calderon et al. (2019) studied the relationship between magnetic field variations and the changes in spectral features of ELF/VLF emissions from conjugated events observed at opposite sides of the magnetosphere. However, reported conjugated cases showing one-to-one correspondence remain rare, with previous studies only being able to discuss wave properties on a case by case basis. Here we present, for the first time, multiple cases of ground and spacecraft observations showing one-to-one correspondence between KAN and the Japanese satellite Exploration in energization and Radiation in Geospace (ERG), more commonly known as Arase. For simplicity, we will use the acronym ERG in the rest of this paper. In this study, we discuss common characteristics and differences between these cases as well as, general wave propagation. Particularly, we found that the ionospheric footprint of ERG was almost systematically located equatorwards (south or south-west) of KAN.

2. Data

We use data from a VLF receiver located in KAN [MLAT = 64.4 N, L = 5.5], Finland, managed by the Sodankyla Geophysical Observatory. The magnetic field variations in the east-west and north-south directions are measured by two separate square loop antennas with a sampling frequency of 78.125 kHz. Further details on the system can be found in Manninen (2005).

We also use data from the ERG spacecraft, with an orbital inclination of 31° and an elliptical orbit with an apogee altitude of 32,000 km (Miyoshi, Shinohara, et al., 2018). Electric and magnetic field data are measured by the Plasma Wave Experiment (Kasahara, Kasaba, et al., 2018). Electric field spectra from 10 Hz to 20 kHz and magnetic field spectra from 1 Hz to 20 kHz with 1 s time resolution (132 frequency points, nominal mode) is provided by the On-board Frequency Analyzer (OFA) (Matsuda et al., 2018). The Magnetic Field Instrument (MGF) is a fluxgate magnetometer measuring low frequency magnetic field variations. Measurements at $L < 4$ have a 256 Hz sampling rate, while for $L > 4$ the sampling rate is 64 Hz (Matsuoka, Teramoto, Nomura, et al., 2018). Upper-hybrid resonance frequency with 1 or 8 s time resolution, depending on observation mode, is obtained from the High Frequency Analyzer (HFA) (Kumamoto et al., 2018). For this study we use 1-min density L3 HFA data.

We use the singular value decomposition (SVD) of spectral matrices described in Santolík et al. (2003) to calculate the angles of the wave vector in relation to the local background magnetic field vector. We then determinate if wave propagation at ERG is oblique or field aligned. From the same SVD method we also obtain planarity (validity of plane wave approximation) and polarization (whistler-mode waves are right-handed polarized waves). The ionospheric magnetic footprint of ERG and L-shells mentioned in this study were calculated using the IGRF internal model and Tsyganenko (T04) external model (Tsyganenko & Sitnov, 2005) unless otherwise indicated.

3. Case Selection

Since KAN operates on a campaign basis, we considered data covering from March 1, 2017 to April 26, 2018, for a total of approximately 9 months of data. We note that there is no data during the summer months (May to August 2017) and, during the campaigns, there are occasional days with disruption of the observations due to technical difficulties. In the study period, KAN was operational for 6,252 h ~260 days. Previous studies focused on efficiently finding ground-space conjugated events suggest that the footprint of the satellite should be located up to 1,000–1,500 km from the station (Martinez-Calderon et al., 2016). Therefore, using the Conjunction Event Finder (CEF) (Miyashita et al., 2011), we selected timings in which the footprint of the satellite was within 1500 km from KAN. We note that the CEF uses the T96 model to calculate these footprints (Tsyganenko & Stern, 1996).

We consider that the timings in which the footprint of ERG is near-by KAN correspond to possible conjunction events. We obtained 483 possible conjunction hours corresponding to only ~8% of the total hours of observations at KAN. We also note that KAN was not operational for 16 h, observed no waves at all for 153 h and observed naturally occurring waves (any type) 67.2% of the time (314 h). During these hours, ERG detected waves (any type) 63.1% of the time (198 h).

We compared the waves observed at KAN and ERG at these timings and found two types of candidates: (1) simultaneous events and (2) conjugated events. For (1), waves showed similar spectral features but different timings or frequencies. For example, both ERG and KAN observed chorus waves but at different frequencies or QP emissions with different periodicity. We found 19 cases of such waves with similar features, spanning over 38 h or 8.2% of the total observation time. Since these waves do not show the same features in the spectra, they are likely being generated by two separated source regions and have distinct propagation properties.

For (2), waves showed the same frequency, spectral and time features (one-to-one correspondence) in both space and ground, suggesting the waves observed at the two locations come from the same source and share common propagation characteristics. In this paper, we will focus on conjugated events with one-to-one correspondence, therefore only criteria (2). We observed 13 conjugated cases between KAN and ERG, spanning ~25 h (5% of possible conjunction hours or 0.4% of total observation hours at KAN). These results emphasize that even with increasing data sets available, ground-space conjugated events showing one-to-one correspondence remain very rare.

Figure 1 shows three examples of conjugated events using 10-min power spectrum density (PSD) obtained from magnetic field variations. For each example, top panel shows observations at KAN and bottom panels at ERG. Figures 1a and 1b show, respectively, a high frequency burst observed simultaneously at ERG and KAN on January 20, 2018 at ~6.5 kHz. Comparing the spectral characteristics we are likely observing the same wave on the ground and in space, or at least waves from the same source. In the same format, Figures 1c and 1d show a QP emission where we can easily see one-to-one correspondence of different QP elements between ~1.5 and 4 kHz. Finally, Figures 1e and 1f show hiss modulated by a QP emission. We see periodic bursts below 1 kHz and a slanted periodic "tip" on top of the hiss at ~1.5 kHz in both locations. Even though conjugated events only represent less than 1% of total available hours, this is the first time such a large number of events of this type has been reported.

4. General Results

The principal characteristics of the 13 one-to-one conjugated events are summarized in Table 1. We list the chronologically numbered cases with their respective date and time of observation, type, maximum, and minimum distance between KAN and ERG footprint, wave-normal angle and the magnetic latitude range (MLAT) at ERG. The wave types are mostly quasiperiodic (QP), but we also observed chorus (C), bursts (B), and hiss (H). One-to-one correspondence of wave features is easier to detect with discrete emissions explaining the high number of QP events. More than half of the events were observed in early 2018 during the winter conjunction fly-by campaign between KAN and ERG. At these times, data are deliberately recorded when ERG is positioned to have its magnetic footprint near KAN, increasing the chances of observing
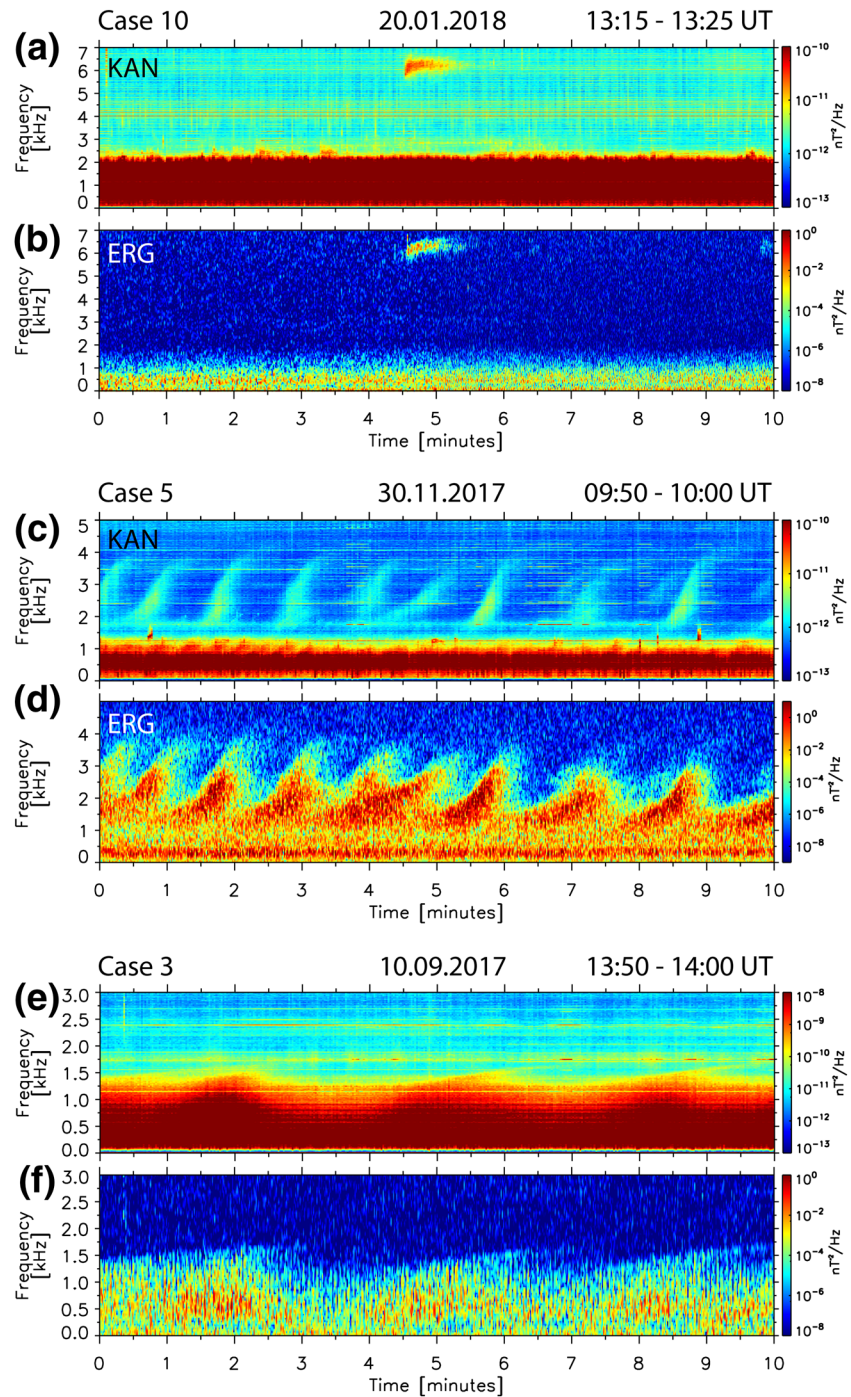
Figure 1. Example of three cases showing one-to-one correspondence between KAN (top in each panel) and ERG (bottom in each panel). (a and b) Case 10 shows a bursty-patch between minutes 4 and 6 at ~6.5 kHz. (c and d) Case 5 is a clear QP emission with a periodicity of ~1 min between 1.5 - 4 kHz. (e and f) Case 3 shows a hiss emission with QP features at ~1.5 kHz. KAN, Kannuslehto; ERG, Exploration in energization and Radiation in Geospace; QP, quasiperiodic.

conjugate events. Duration of the events varies from a few minutes up to 3 h, with an average of 40–50 min. Case 8 is particular because of missing data at KAN not allowing us to accurately determine the start of the event, meaning timings here are those recorded at ERG. While we consider that the end of the one-to-one correspondence at one location indicates the end of the conjugated events in several occasions at least one

Table 1
Summary of all 13 One-to-one conjugated cases considered in this study From left to right: case number, observation date and times, type of emission (C: chorus, QP: quasiperiodic, (H) hiss, (B) bursts), maximum frequency, minimum and maximum distance between ERG footprint and KAN, wave-normal angle (O: oblique ≥20°, FL: field aligned < 20°), Magnetic latitude and L-shell at ERG, and magnetic local time of observation. MLT at KAN is UT + 1.5 hr. Start and end times indicate timings of one-to-one correspondence between KAN and ERG.

Case	Date	Start (UT)	End (UT)	Type	f_{max} (kHz)	D Min/Max (km)	$\bar{k}$ at ERG	MLAT (°)	L at ERG (R_E)	MLT (h)
1	March 28, 2017	22:35	23:05~	C/QP	2.0	76/612	FL	−28 to −24	4.57 to 5.26	0.97 to 1.73
2	March 30, 2017	21:57	22:12	C	2.5	201/261	FL	−28 to −26	4.69 to 5.05	0.97 to 1.38
3	September 10, 2017	13:24	14:35	H/QP	1.6	333/2,332	O	+9 to +23	2.45 to 4.40	14.56 to 16.56
4	November 28, 2017	12:10	12:59	H/QP	1.3	264/466	O[a]	+21 to +19	6.32 to 6.54	15.03 to 15.58
5	November 30, 2017	09:30	10:22	QP	4.1	323/962	O to FL	+28 to +24	3.77 to 5.07	12.03 to 13.82
6	December 26, 2017	10:00	12:10	QP	2.0	73/2043	O to FL	+30 to +17	4.04 to 5.28	10.72 to 12.72
7	January 7, 2018	11:56	12:40	QP	4.0	182/333	O to FL[a]	−10 to −16	5.20 to 4.60	14.83 to 15.42
8	January 18, 2018	06:00	08:50~	QP	4.0	864/2,089	O[a]	+28 to +6	1.33 to 1.89	2.84 to 4.84
9	January 18, 2018	13:34	15:00~	QP	6.0	864/2,500	FL to O[a]	−16 to −38	4.57 to 3.32	14.61 to 16.61
10	January 20, 2018	13:19	13:21	B	7.0	1,140/1,153	O	−22 to −23	4.18 to 4.14	15.04 to 15.09
11	January 20, 2018	13:29	13:30	B	7.0	1,111/1,125	O	−25 to −26	3.98 to 3.96	15.32 to 15.35
12	January 22, 2018	06:32	06:57	QP	1.5	936/1,163	FL[a]	+10 to +7	4.71 to 5.08	10.76 to 11.16
13	February 2, 2018	14:00	14:32	H/QP	2.0	1,078/1,628	O to FL	−30 to −37	3.67 to 2.94	15.14 to 17.14

From left to right: case number, observation date and times, type of emission (C: chorus, QP: quasiperiodic, (H) hiss, (B) bursts), maximum frequency, minimum and maximum distance between ERG footprint and KAN, wave-normal angle (O: Oblique ≥ 20°, FL: Field Aligned < 20°), magnetic latitude and L-shell at ERG, and magnetic local time of observation. MLT at KAN is UT + 1.5 h. Start and end times indicate timings of one-to-one correspondence between KAN and ERG.
[a]Low planarity, <0.5.

location observes waves longer. In most cases, the waves are observed longer at KAN, sometimes up to several hours. Cases 3 and 7 are the only ones where the waves continued to be observed for 20–30 min longer on-board ERG.

On first approach, the duration of the events inversely correlates with geomagnetic activity. Events longer than an hour were observed when AE < 200 nT and average Dst > −30 nT. Most events happened during the recovery phase of storms and generally under quiet conditions. We speculate that at times of low geomagnetic activity, even though wave generation is usually weaker, waves reach the ground more easily. However, a superposed epoch analysis of the geomagnetic and solar wind conditions, where the zero-epoch was the starting time of the emissions in this study, did not yield conclusive results. A much larger number of events is needed to further discuss any relationship between these two elements.

In general, conjugated events were observed when ERG was 20–30° of latitude from the geomagnetic equator. Wave-normal angles at ERG were mostly oblique, with a few field-aligned cases. Previous ray tracing simulations suggested that as the wave moves away from the equatorial source region, wave refraction caused by magnetic gradients and curvatures makes the wave-normal angle become more oblique at higher latitudes (Breneman et al., 2009; Chen et al., 2013; Horne & Thorne, 2003). A study of chorus wave-normal angles based on 11 years of measurements of the Cluster spacefleet show that wave-normal angles still tend to remain field aligned (Santolík et al., 2014); a possible explanation by a system of small ducts has been recently demonstrated by Hanzelka and Santolík (2019).

The average equatorial half-gyrofrequency (f_{ce}) for electrons at the L-shell of KAN is ~2 kHz. Although the maximum frequency of the waves at KAN was sometimes between 0.5 f_{ce} and f_{ce}, waves corresponding to the lower band (<0.5 f_{ce}) were the most frequently observed. In three cases, maximum wave frequency was above f_{ce}, two of those correspond to high frequency short-time bursts (Cases 10 and 11). The observations of these type of high frequency bursts are possible at KAN thanks to an innovative sferics filtering system, allowing clear observations at frequencies otherwise dominated by sferics noise (Manninen et al., 2016).
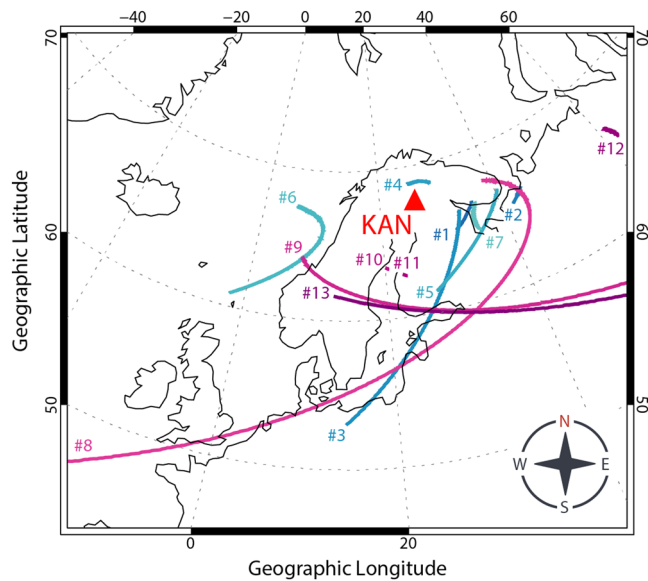
Figure 2. Location of the satellite's ionospheric magnetic footprint calculated using T04 in respect to the ground station (red triangle). Warm lines indicate events that happened during the conjunction campaigns between ERG and KAN. KAN, Kannuslehto; ERG, Exploration in energization and Radiation in Geospace.

In general, ERG was at slightly lower L-shells compared to KAN (L = 5.5, IGRF model only). The mean L-shells of observation at ERG for all cases vary between 1.41 and 6.15, with the highest value corresponding to Case 4 (ERG footprint north of KAN). The average L-shell of observation was L = 4.57 with 10 cases observed at $4.2 < L < 5.5$.

MLT distribution of the events shows that 90% of the cases were observed on the day side (afternoon sector, 13–17 MLT). During the considered time frame, ERG covered most MLT sectors with some hours missing in the morning side. High number of observations on the dayside is therefore not related to the position or coverage of the spacecraft. Occurrence rate in relation to the total possible conjunction hours on the dayside (6–17 MLT) and nightside (18-5 MLT), was, respectively 4% ±1 and 0.008% ± 0.004%. Dayside occurrence being 500 times more likely than nightside explains that most cases were detected in the afternoon MLT. Additionally, it is also easier to identify one-to-one correspondence between waves that have distinct elements and, accordingly, a majority of the cases shown here are QP emissions. These type of waves are known to be a dayside phenomenon (Engebretson et al., 2004; Hayosh et al., 2014; Martinez-Calderon et al., 2015b; Sato et al., 1974).

5. Discussion on Likely Location of the Ionospheric Exit Point

5.1. Location of the Satellite Ionospheric Footprint

Table 1 shows that, on average, the distance D between KAN and the ionospheric footprint of ERG is <1,000 km. However, in several cases the waves were observed at much larger distances. In at least four cases, they were detected up to ~2,000 km from the KAN with a maximum of 2,500 km (Case 9). These new larger distances should be considered in future research of simultaneous or conjugated events. Figure 2 shows the footprint of ERG for all 13 cases in relation to the location of the ground station (red triangle). Each case number is shown at the start of the footprint. Cold colors indicate cases before the ERG/KAN conjunction campaign, while warm colors show those observed during the campaign. The footprint for the cases during the ERG/KAN campaign are usually located closer to KAN. For cases 3, 9, 8, and 13, the ionospheric footprint of ERG sweeps from west to east, but always south of KAN. For cases 1, 2, 7, and 5 and 12, the footprint was south-east of KAN, while for cases 6, 10, and 11, it was located south-west of the station. Figure 2 shows clearly that the footprint of ERG is consistently south of KAN, with no clear east/west pattern.

5.2. Direction of Incoming Waves at KAN

While the location of ERG can give some information on how the wave propagated, we are interested in locating the point where the waves exited the ionosphere, i.e., the ionospheric exit point. Previous studies of simultaneously observed chorus emissions between two ground stations and during different geomagnetic conditions, found that this exit point was in the same area throughout the duration of the emissions (Martinez-Calderon et al., 2015b). Similarly, Martinez-Calderon et al. (2019) found that the exit point of two conjugated events was south of KAN, and within 100 km of each other. On the other hand, Demekhov et al. (2017) reported a chorus conjugated event between KAN and RBSP-A where the footprint of the satellite was eastwards of the station.

Focusing on polarization analysis, Ozaki et al. (2008) found that polarization gradually changes from right-handed to linear and then left-handed as the horizontal distance becomes larger from the injection point of the waves in the ionosphere and the waves are allowed to bounce in the Earth-ionosphere wave guide. If the waves at KAN are detected as left-handed it means they do not come straight from the ionosphere. In this study, all waves at KAN are right-handed, thus exiting the ionosphere directly from an exit point close to the receiver (within ~250 km).
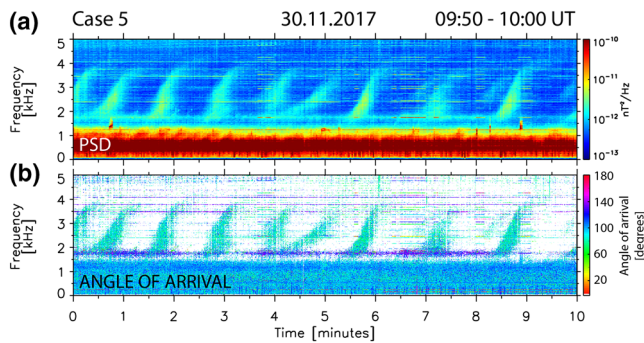
Figure 3. (a) PSD of 10 min of case 5 at KAN showing a QP emission between 1.5 and 4 kHz, and (b) the corresponding angle of arrival indicating the direction the waves were detected at KAN (0° and 180° indicate the north-south direction). PSD, power spectrum density; KAN, Kannuslehto. QP, quasiperiodic .

Using the angle between the minor axis of the polarization ellipse of the waves and the north-south direction, we inferred the direction of arrival of the waves at KAN with an ambiguity of 180° (0° or 180° indicates the north-south direction) (Hayashi et al., 1968; Manninen, 2005; Martinez-Calderon et al., 2015a). Figure 3a shows 10-min PSD of the QP emission for case 5 at KAN, and Figure 3b the corresponding angle of arrival with values between light green to cyan, corresponding to 70° and 90°.

We compared this angle of arrival to the position of the ionospheric footprint of ERG. In the following discussion, we consider the minimum and maximum values of the angle of arrival for the entire duration of each case, and assumed this indicates the location of the ionospheric exit point. In all the cases, the waves were right hand polarized at KAN inferring they exited directly the ionosphere to the station, and thus the exit point should be within a few hundred km of the station. Figure 4 shows, for each case, the position of the footprint of ERG and the direction where the waves were detected at KAN. Orange arcs indicate maximum and minimum angles of arrival for a circle of ~250 km from the ground station (red triangle).

While we cannot speculate on the actual location of the emission source, we can reasonable assume that whistler-mode waves propagating along the magnetic field line at KAN would be propagating below 0.5 f_{ce} on that field line (~2.5 kHz). At lower L-shells, south of KAN, this frequency increases. As KAN does not provide electric field data, we have an 180° ambiguity of the angle of arrival, meaning in some cases we show two possible directions with two orange arcs.

For cases, 1, 2, 7, 10, and 11 the waves were detected either from the south-west or north-east of KAN. As the observed wave frequency was above 2.5 kHz, it is likely they were coming from the south-west direction (Figure 4). For cases 10 and 11, this correlates with the direction of the footprint of ERG. On the other hand, for cases 1, 2, and 7, the footprint was in another direction, south-east of KAN. The angle of arrival gives us the likely location of the ionospheric exit point, south-west of KAN, while the position of ERG suggests that the waves were moving westwards as they traveled to the ground.

Cases 8 and 9 had a south-west angle of arrival, shifting westwards in time. This shift is represented by the orange (earlier values) to dark orange (latter values) arcs in Figure 4. The footprint of the satellite was moving from west to east suggesting ERG kept observing the waves as it moved eastwards. We can explain this by assuming a large longitudinally extended source region. Cases 8 and 9 are both QP emissions and several studies on the spatial extent of the source region of these waves have hinted at a longitudinally extended QP source (e.g., Martinez-Calderon et al., 2020; Němec, Bezděková, et al., 2016; Němec et al., 2018; Němec, Hospodarsky, et al., 2016). Even if the waves were generated by a large source region, they could have only penetrated the ionosphere south-west or west of KAN. The angle of arrival indicates that the ionospheric exit point moves westwards with time, therefore assuming a longitudinally extended source, this result implies changes in the ionospheric composition are making the ionosphere slowly penetrable westwards from KAN.

For case 5, waves were detected from either the east or west while the footprint of ERG was south-east from KAN. Assuming a large source region, the exit point could be west of KAN, in the opposite direction of ERG. However, the exit point could also be closer to the position of the satellite, and therefore east of KAN. We can only conclude that it was likely located at higher latitudes than the footprint of ERG.

For the rest of the cases, 3–6 and 12–13, the angle of arrival was south-west or north-east of KAN. For cases 4 and 13, this suggests the exit point is located respectively, south or north of the footprint of ERG, and likely closer to the station in either the east or west direction. For cases 3, 6, and particularly, 12, this result puts the exit point farther away from the footprint of the satellite and possibly in the opposite direction from KAN. As discussed above, this could also be the result of a longitudinally extended source region, however another explanation could be the meridional expansion of the waves during propagation (Section 6.1, Figure 6).
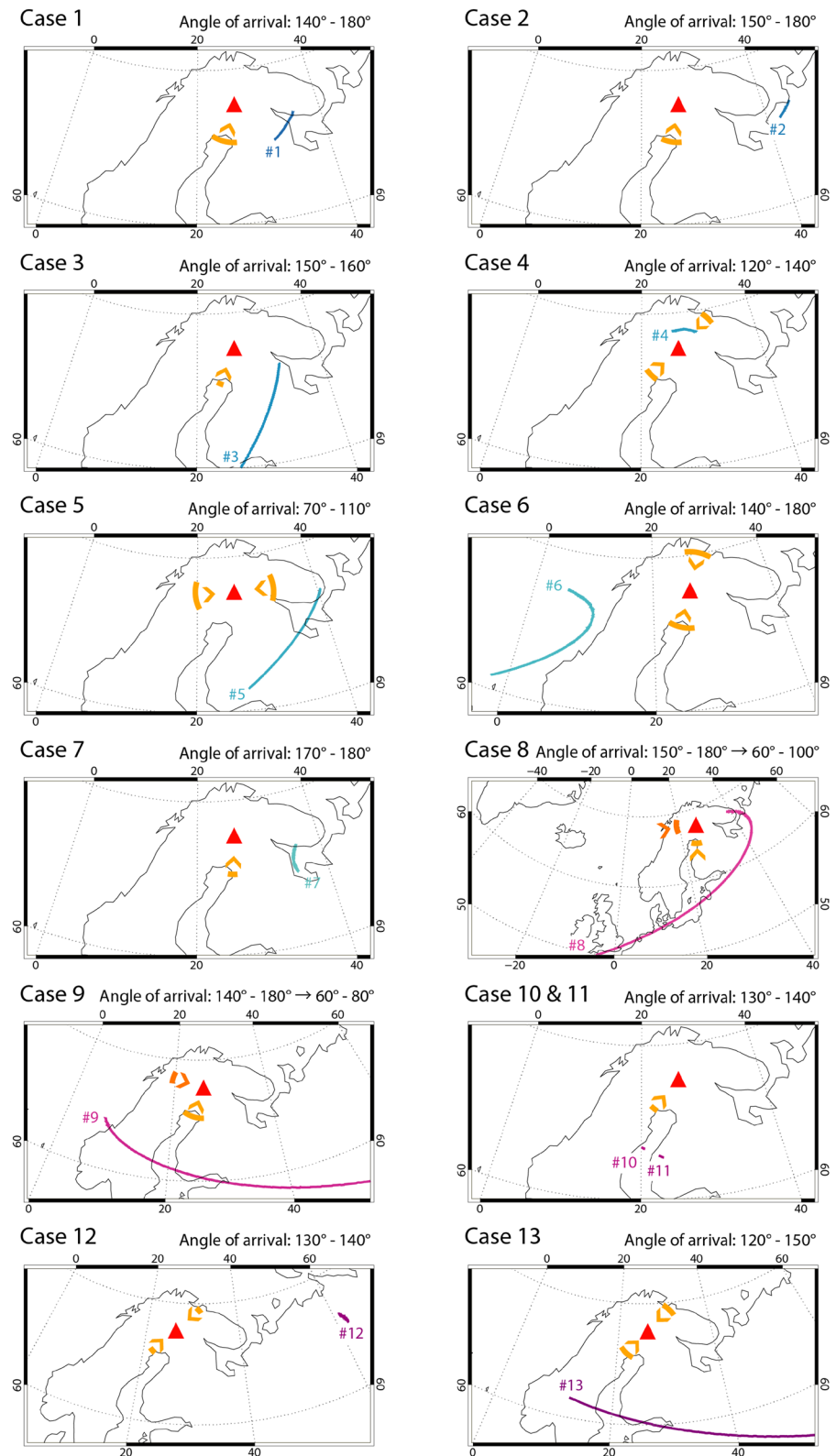
Figure 4. Location of ERG's ionospheric magnetic footprint in respect to KAN (red triangle) and angle of arrival detected at KAN. Orange arcs indicate the approximate incoming direction of the waves estimated from the angle of arrival (indicated on top of each case, example in Figure 3) at a maximum of 250 km from KAN. Arrows indicate the direction of the waves. Shifting colors from orange to dark orange indicate changes of the angle with time. ERG, Exploration in energization and Radiation in Geospace; KAN, Kannuslehto.

5.3. Influence of Density in Ionospheric Exit Point Movements

As we expect the ionospheric exit point to be within 250 km from KAN, we found that in a little over half of the cases this point was located between the station and the footprint of the satellite. Figure 5 shows density measured by ERG along the spacecraft orbit ±2 h MLT from the start of each event. Gray overlay shows the duration of the conjugated event for each case. We note that in some cases the ending time of the event is beyond the time frame shown here. For cases 8 and 9, we observe, respectively, slow smooth decrease and increase of the density along the path of ERG. As these cases lasted 2–3 h, the ionospheric exit point could have moved westwards in time due to gradual changes in background plasma composition, or to changes in the propagation of the waves at the source. The angle of arrival for case 5 was east or west of KAN. Comparing it to the location of ERG, we suggest that the exit point was eastwards, at higher latitudes than the footprint of the satellite.

6. Discussion on Wave Propagation and Properties

The path of the footprint of ERG for cases 9 and 13 is very similar (Figure 2). However, while both cases are discrete, we found no resemblance in their spectral features or the frequencies. The footprints for cases 1, 2, 3, 5, and 7 are in the same region south-east of KAN. Similarly, while these cases show QP characteristics, they do not share any other specific properties. We found no correlation between wave intensity and distance to the satellite footprint or likely location of the ionospheric exit point. We conclude there is no significant relation between the position of ERG and the type of emissions or intensity of the conjugated events.

Although a majority of the cases where in the same afternoon MLT sector, they were observed during different geomagnetic conditions, with an average AE of 40–800 nT and Dst of −50 to 20 nT. Even if the events happened under different conditions, the satellite usually observed them in a similar region of space, and ~20°off equator. We previously noted that the ionospheric exit point was generally south of KAN, suggesting a privileged propagation "highway" with high likelihood of reaching the ground. Otherwise, the location of ERG for different cases would be significantly more random.

6.1. Density and Wave Propagation in the Magnetosphere

The propagation time of VLF waves from the magnetosphere to the ionosphere is of the order of a few seconds, meaning that on the scale of wave propagation the Earth is considered as completely still. Propagation effects should then come from the medium, either from the magnetic field or background plasma density. In general, the magnetic field is symmetric particularly at low L-shell suggesting that this observational result is most likely due to plasma density. Therefore, we investigated density variations along the path of ERG. Figure 5 shows these density measurements ±2 h MLT from the start of each event. Gray overlay represents event duration, noting sometimes the ending of the event is beyond the time frame shown here. We indicate MLT, L-shell, altitude and MLAT for each case

For cases in green (1–6, 8, and 12), ERG was moving to regions of lower plasma density, while cases in black (7, 9, 10–11, and 13) correspond to movement to higher densities. L-shell and altitude show that for green cases, ERG was moving outwards while for black cases it was moving inwards. The variations of background plasmaspheric density greatly depend on the radial motion of the satellite, as the radial gradient of density is much higher than the longitudinal gradient. In cases 3, 5, and 9, ERG is moving inwards (outwards) across several L-shells reaching regions of naturally higher (lower) plasma density. In cases 2 and 4, the density remains stable even though ERG is moving across a distance of ~0.5 L. In all these cases, smaller and rapid density variations were observed periodically through out the duration of the conjugated event, indicating ducted propagation to the ground (Haque et al., 2011; Martinez-Calderon et al., 2016; Smith et al., 1960). However, since the size of the duct is much smaller than the overall duration of the event, it is more likely than the waves were generally propagating unducted, with occasional ducting, maybe with a larger number of small-case ducts with a lower density variation (Hanzelka & Santolík, 2019). For Cases 1, 6, 8, and 12 ERG moved less than 0.5 L radially (<3,000 km) with steady density decrease (up to 1 order of magnitude for case 1). This is clearer in case 6 where ERG barely moved within 0.1 L with continuing plasma decrease. Cases 1 and 6 show possible ducted propagation at specific intervals during the conjugated event, while for
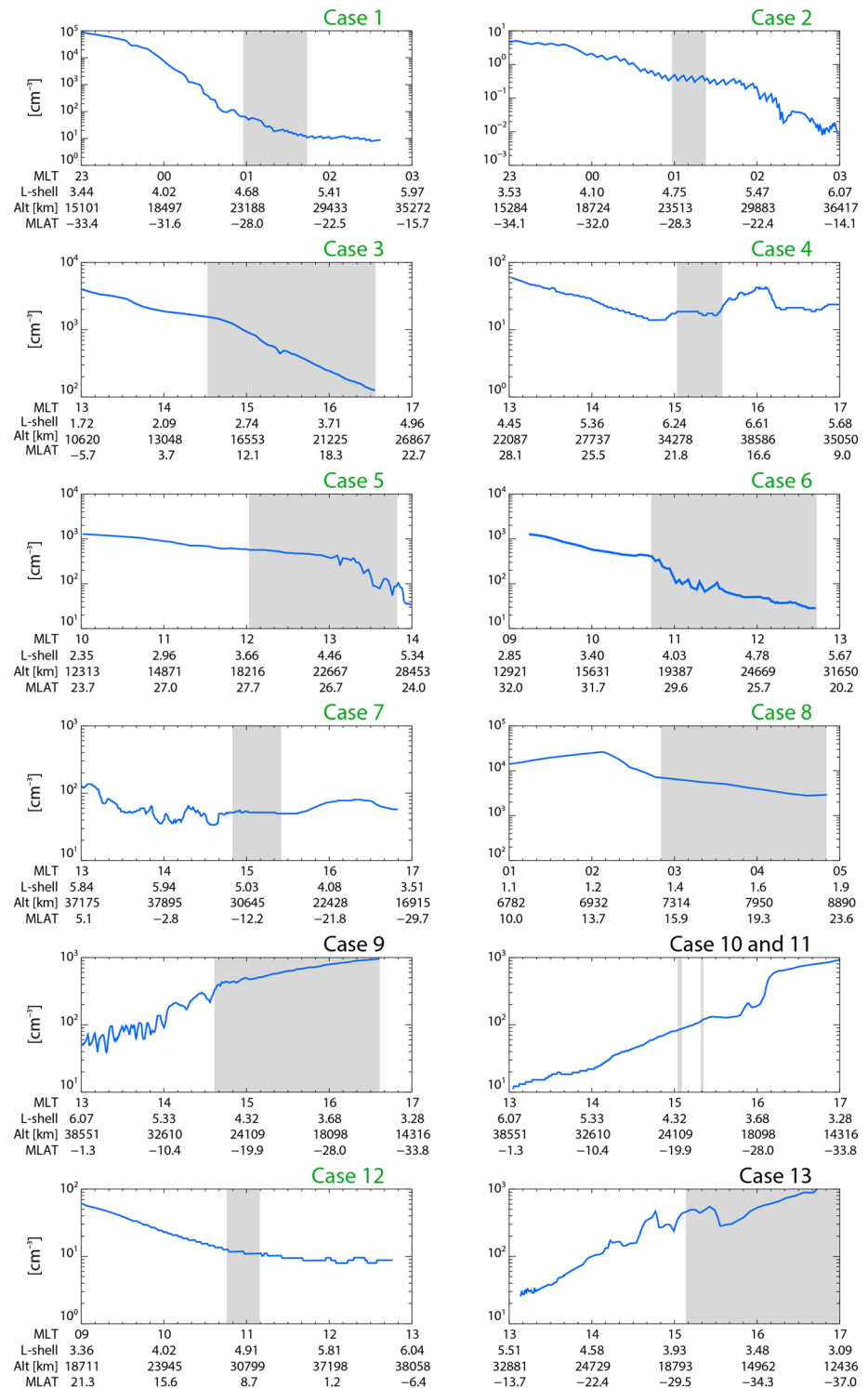
Figure 5. Plasma density measured by ERG for Cases 1–13 as a function of MLT, 2 h before and after the start of the conjugated events. Gray overlay indicates the timing of the conjugated event for each case. Green (black) show cases where the satellite was moving to regions of lower (higher) plasma density. ERG, Exploration in energization and Radiation in Geospace.
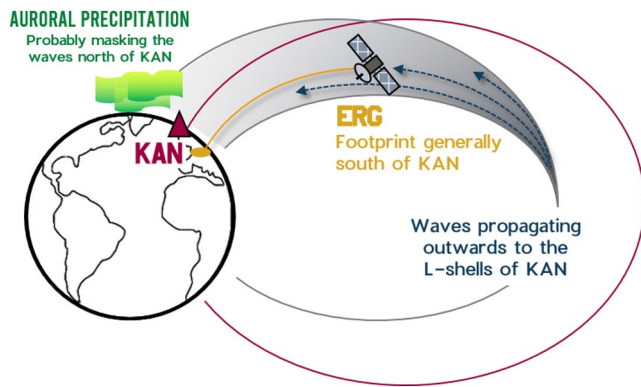
Figure 6. Schematic figure (not to scale) illustrating the likely propagation path of the waves observed in the 13 conjugated cases. Waves were found to propagate largely unducted, outwards to the L-shells of KAN. In some cases, we believe that auroral precipitation at higher latitudes stopped the waves for penetrating the ionosphere north of KAN. KAN, Kannuslehto.

cases 8 and 12 the waves likely propagated unducted. Cases 10 and 11 correspond to very short bursts of VLF waves. Since they are only a few minutes long, we consider that there is not enough time for changes in density to affect the propagation of the waves and variations in density do not show any density ducts. Similarly, case 13 has a relatively short duration, however small changes in plasma density during the entire event suggest ducted propagation.

Our results show no systematic propagation manner with most cases suggesting predominant unducted propagation from the source to KAN. The ionospheric footprint of ERG was usually south of KAN, at lower L-shells, suggesting waves coming from the magnetosphere to the ionosphere tend to propagate outwards to higher L-shells, rather than inwards (Figure 6). Analysis on the probable location of the ionospheric exit point of waves near KAN and the position of ERG suggest VLF waves have a rather large or longitudinally extended source region. This has previously been suggested by Martinez-Calderon et al. (2020), Němec et al. (2016, 2018), Němec, Bezděková, et al. (2016), and Němec, Hospodarsky, et al. (2016). Although at this stage we cannot speculate on the actual source location of the waves, we found there is a clear tendency in our observations. Ideally, a more thorough analysis including ray tracing could help elucidate these differences and confirm our hypothesis.

As the density gradient of the plasmapause can trap the VLF wave energy (Inan & Bell, 1977), we used density data from HFA to approximate the location of the plasmapause closest to each event time. Generally, the events were observed outside of the plasmasphere, between 30 min and 1 h after the outbound crossing. In cases 5, 8, and 9, the plasmapause was difficult to determine. However, the data suggests that the emissions happened while ERG was inside the plasmasphere, or within a very wide plasmapause. Shortly after, ERG crossed the plasmapause the waves were no longer observed. For cases 3 and 6, the events started close to the plasmapause on the outbound crossing, suggesting these waves might have been guided to the ground, as proposed by Hanzelka et al. (2017).

6.2. Effect of Particle Precipitation on Ionospheric Wave Propagation

Previous studies have shown that precipitating electrons can produce localized secondary ionization and conductivity enhancements. If this ionization enhancement extends into the D-region of the ionosphere, then VLF emissions propagating in the earth-ionosphere waveguide can see their amplitude and phase disrupted (e.g., Helliwell et al., 1973; Inan et al., 1984, 1985; Ozaki et al., 2009). Therefore, precipitation in the auroral region at higher latitudes than KAN, should affect wave propagation. This suggests waves propagating poleward from KAN might be unable to penetrate the ionosphere due to higher plasma density in the auroral region. The location of the footprint of ERG southwards of KAN can be the consequence of VLF waves being masked by the auroral ionosphere at higher latitudes (Figure 6). Several cases presented here were observed during periods of low to moderate geomagnetic activity supporting this idea. However, cases 4 and 12, with the most northwards footprints, were observed during the expansion phase of moderate substorms (AE ~400 nT), indicating that during relatively higher ionization periods waves can still penetrate the ionosphere north of KAN. Additional studies showing the existence of waves when ERG is located northwards of KAN while the station does not detect waves are necessary to understand and quantify the extent of this effect.

7. Summary

Although by their nature, conjugated events give us significant information on the generation and propagation of waves, up until now they remain rare with only a handful of documented cases. We presented here 13 conjugated events showing one-to-one correspondence between a ground VLF receiver located in Northern Finland and the ERG satellite in the inner magnetosphere.

We found that most cases were observed in the afternoon MLT, during the recovery phase of storms and under generally quiet conditions, suggesting that it is easier for the waves to propagate to the ground under these conditions. After the end of the events, the emissions were usually still observed at KAN for up to 30 min. ERG was usually located close to the equator, and at slightly lower L-shells than KAN. We found that while all these cases were observed at different timings and slightly different geomagnetic conditions, the waves seemed to exit the ionosphere to the ground at similar locations and almost systematically south of KAN. This can be due to the waves not being able to exit the ionosphere at higher latitudes than KAN because they are being masked by precipitation linked to auroral activity. Using the angle of arrival at KAN and the position of the footprint of ERG we also estimated the likely position of the ionospheric exit point which seemed to be usually located between the footprint and the station. Using the measurements of background plasma density, we investigated the propagation of the waves from the magnetosphere to the ground. We found that the waves were mostly propagating unducted, and likely from an inner source outwards to the L-shells of KAN. While preliminary observations may suggest a favored path from the source region, using only the ERG density data we were unable to find a common density structure to all the cases to determine that this was the case. Further analysis of wave propagation using ray tracing might be able to provide more insight into this point.

Data Availability Statement

Science data of the ERG (Arase) satellite were obtained from the ERG Science Center operated by ISAS/JAXA and ISEE/Nagoya University (https://ergsc.isee.nagoya-u.ac.jp/index.shtml.en, Miyoshi, Hori, et al., 2018). ERG satellite datasets for this research are available in these in-text data citation references: Kasahara, Kojima, et al. (2018), Kasahara, Kumamoto, et al. (2018), Matsuoka, Teramoto, Imajo, et al. (2018), Miyoshi, Shinohara, and Jun (2018). The present study analyzed MGF v03.03 data, PWE OFA v02.01 data (including OFA-Matrix), PWE HFA-L2 v01.01 data and PWE HFA-L3 v.01.02 data. VLF data is available at https://www.sgo.fi/pub_vlf/ for KAN and specific datasets for this research are available in this in-text data citation reference: Martinez-Calderon and Manninen (2020).

References

Barr, R., Jones, D. L., & Rodger, C. (2000). ELF and VLF radio waves. *Journal of Atmospheric and Solar-Terrestrial Physics*, *62*(17), 1689–1718.

Bortnik, J., & Thorne, R. (2007). The dual role of ELF/VLF chorus waves in the acceleration and precipitation of radiation belt electrons. *Journal of Atmospheric and Solar-Terrestrial Physics*, *69*(3), 378–386.

Breneman, A. W., Kletzing, C. A., Pickett, J., Chum, J., & Santolik, O. (2009). Statistics of multispacecraft observations of chorus dispersion and source location. *Journal of Geophysical Research*, *114*, A06202. https://doi.org/10.1029/2008JA013549

Chen, L., Thorne, R. M., Li, W., & Bortnik, J. (2013). Modeling the wave normal distribution of chorus waves. *Journal of Geophysical Research: Space Physics*, *118*, 1074–1088. https://doi.org/10.1029/2012JA018343

Demekhov, A. G., Manninen, J., Santolík, O., & Titova, E. E. (2017). Conjugate ground-spacecraft observations of VLF chorus elements. *Geophysical Research Letters*, *44*, 11735–11744. https://doi.org/10.1002/2017GL076139

Engebretson, M., Posch, J., Halford, A., Shelburne, G., Smith, A., Spasojević, M., & Arnoldy, R. (2004). Latitudinal and seasonal variations of quasiperiodic and periodic VLF emissions in the outer magnetosphere. *Journal of Geophysical Research*, *109*, A05216. https://doi.org/10.1029/2003JA010335

Hanzelka, M., & Santolík, O. (2019). Effects of ducting on whistler mode chorus or exohiss in the outer radiation belt. *Geophysical Research Letters*, *46*, 5735–5745. https://doi.org/10.1029/2019GL083115

Hanzelka, M., Santolík, O., Hajoš, M., Němec, F., & Parrot, M. (2017). Observation of ionospherically reflected quasiperiodic emissions by the demeter spacecraft. *Geophysical Research Letters*, *44*, 8721–8729. https://doi.org/10.1002/2017GL074883

Haque, N., Inan, U. S., Bell, T. F., Pickett, J. S., Trotignon, J.-G., & Facskó, G. (2011). Cluster observations of whistler mode ducts and banded chorus. *Geophysical Research Letters*, *38*, L18107. https://doi.org/10.1029/2011GL049112

Hayashi, K., Kokubun, S., & Oguti, T. (1968). *Polar chorus emission and worldwide geomagnetic variation. (Tech. Rep. 149–60)*. Tokyo, Japan: Tokyo University.

Hayosh, M., Nemec, F., Santolik, O., & Parrot, M. (2014). Statistical investigation of VLF quasiperiodic emissions measured by the demeter spacecraft. *Journal of Geophysical Research: Space Physics*, *119*, 8063–8072. https://doi.org/10.1002/2013JA019731

Hayosh, M., Pasmanik, D. L., Demekhov, A. G., Santolik, O., Parrot, M., & Titova, E. E. (2013). Simultaneous observations of quasi-periodic ELF/VLF wave emissions and electron precipitation by demeter satellite: A case study. *Journal of Geophysical Research: Space Physics*, *118*, 4523–4533. https://doi.org/10.1002/jgra.50179

Helliwell, R. A., Katsufrakis, J. P., & Trimpi, M. L. (1973). Whistler-induced amplitude perturbation in VLF propagation. *Journal of Geophysical Research*, *78*, 4679–4688

Horne, R., & Thorne, R. (2003). Relativistic electron acceleration and precipitation during resonant interactions with whistler-mode chorus. *Geophysical Research Letters*, *30*(10), 1527. https://doi.org/10.1029/2003GL016973

Horne, R. B., Thorne, R. M., Shprits, Y. Y., Meredith, N. P., Glauert, S. A., Smith, A. J., & Decreau, P. M. E. (2005). Wave acceleration of electrons in the van Allen radiation belts. *Nature*, *437*(7056), 227–230. http://doi.org/10.1038/nature03939

Inan, U. S., & Bell, T. F. (1977). The plasmapause as a VLF wave guide. *Journal of Geophysical Research*, *82*(19), 2819–2827.

Inan, U. S., Carpenter, D. L., Helliwell, R. A., & Katsufrakis, J. P. (1985). Subionospheric VLF/LF phase perturbations produced by lightning-whistler induced particle precipitation. *Journal of Geophysical Research*, *90*(A8), 7457–7469.

Inan, U. S., Chang, H. C., & Helliwell, R. A. (1984). Electron precipitation zones around major ground-based VLF signal sources. *Journal of Geophysical Research: Space Physics*, *89*(A5), 2891–2906.

Kasahara, Y., Kasaba, Y., Kojima, H., Yagitani, S., Ishisaka, K., Kumamoto, A., et al. (2018). The plasma wave experiment (PWE) on board the Arase (ERG) satellite. *Earth Planets and Space*, *70*(1), 86.

Kasahara, Y., Kojima, H., Matsuda, S., Ozaki, M., Yagitani, S., Shoji, M., & Shinohara, I. (2018). *The PWE/OFA instrument level-2 spectrum data of exploration of energization and radiation in geospace (ERG) Arase satellite*. Nagoya, Japan:ERG Science Center, Institute for Space-Earth Environmental Research, Nagoya University. https://doi.org/10.34515/DATA.ERG-08000

Kasahara, Y., Kumamoto, A., Tsuchiya, F., Matsuda, S., Shoji, M., Nakamura, S., & Miyoshi, Y. (2018c). The PWE/HFA instrument level-2 spectrum data of exploration of energization and radiation in geospace (ERG) Arase satellite. Nagoya, Japan:ERG Science Center, Institute for Space-Earth Environmental Research, Nagoya University. https://doi.org/10.34515/DATA.ERG-10000

Kennel, C. F., & Petschek, H. (1966). Limit on stably trapped particle fluxes. *Journal of Geophysical Research*, *71*(1), 1–28.

Kumamoto, A., Tsuchiya, F., Kasahara, Y., Kasaba, Y., Kojima, H., Yagitani, S., et al. (2018). High frequency analyzer (HFA) of plasma wave experiment (PWE) onboard the Arase spacecraft. *Earth Planets and Space*, *70*(1), 82.

Kurth, W., De Pascuale, S., Faden, J., Kletzing, C., Hospodarsky, G., Thaller, S., & Wygant, J. (2015). Electron densities inferred from plasma wave spectra obtained by the waves instrument on van Allen probes. *Journal of Geophysical Research: Space Physics*, *120*, 904–914. https://doi.org/10.1002/2014JA020857

Li, W., Bortnik, J., Thorne, R., & Angelopoulos, V. (2011). Global distribution of wave amplitudes and wave normal angles of chorus waves using themis wave observations. *Journal of Geophysical Research*, *116*, A12205. https://doi.org/10.1029/2011JA017035

Lyons, L. R., Thorne, R. M., & Kennel, C. F. (1972). Pitch-angle diffusion of radiation belt electrons within the plasmasphere. *Journal of Geophysical Research*, *77*(19), 3455–3474.

Manninen, J. (2005). *Some aspects of ELF-VLF emissions in geophysical research (Doctoral dissertation)*, Oulu, Finland: Sodankylä Geophysical Observatory Publications, Oulu University Press. Retrieved from http://www.sgo.fi/Publications/SGO/thesis/ManninenJyrki.pdf

Manninen, J., Turunen, T., Kleimenova, N., Rycroft, M., Gromova, L., & Sirviö, I. (2016). Unusually high frequency natural VLF radio emissions observed during daytime in northern Finland. *Environmental Research Letters*, *11*(12), 124006.

Martinez-Calderon, C., Katoh, Y., Manninen, J., Kasahara, Y., Matsuda, S., Kumamoto, A., & et al.(2019). Conjugate observations of dayside and nightside VLF chorus and QP emissions between Arase (ERG) and Kannuslehto, Finland. *Journal of Geophysical Research: Space Physics*, *125*, e2019JA026663. https://doi.org/10.1029/2019JA026663

Martinez-Calderon, C., & Manninen, J. (2020). *KAN dataset—Multi-event study of characteristics and propagation of naturally occurring ELF/VLF waves using high-latitude ground observations and conjunctions with the Arase satellite, V1*. Mendeley Data. Retrieved from http://dx.doi.org/10.17632/hg98yvjwtd.1

Martinez-Calderon, C., Němec, F., Katoh, Y., Shiokawa, K., Kletzing, C., Hospodarsky, G., & Kurkin, V. I. (2020). Spatial extent of quasiperiodic emissions simultaneously observed by Arase and van Allen probes on 29 November 2018. *Journal of Geophysical Research: Space Physics*, *125*, e2020JA028126. https://doi.org/10.1029/2020JA028126

Martinez-Calderon, C., Shiokawa, K., Miyoshi, Y., Keika, K., Ozaki, M., Schofield, I., & Kurth, W. S. (2016). ELF/VLF wave propagation at subauroral latitudes: Conjugate observation between the ground and van Allen probes A. *Journal of Geophysical Research: Space Physics*, *121*,5384–5393. https://doi.org/10.1002/2015JA022264

Martinez-Calderon, C., Shiokawa, K., Miyoshi, Y., Ozaki, M., Schofield, I., & Connors, M. (2015a). Polarization analysis of VLF/ELF waves observed at subauroral latitudes during the VLF-chain campaign. *Earth Planets and Space*, *67*(1), 1–13.

Martinez-Calderon, C., Shiokawa, K., Miyoshi, Y., Ozaki, M., Schofield, I., & Connors, M. (2015b). Statistical study of ELF/VLF emissions at subauroral latitudes in athabasca, canada. *Journal of Geophysical Research: Space Physics*, *120*, 8455–8469. https://doi.org/10.1002/2015JA021347

Matsuda, S., Kasahara, Y., Kojima, H., Kasaba, Y., Yagitani, S., Ozaki, M., et al. (2018a). Onboard software of plasma wave experiment aboard Arase: Instrument management and signal processing of waveform capture/onboard frequency analyzer. *Earth Planets and Space*, *70*(1), 75.

Matsuoka, A., Teramoto, M., Imajo, S., Kurita, S., Miyoshi, Y., & Shinohara, I. (2018b). The MGF instrument level-2 spin-fit magnetic field data of exploration of energization and radiation in geospace (ERG) Arase satellite. Nagoya, Japan: ERG Science Center, Institute for Space-Earth Environmental Research, Nagoya University. https://doi.org/10.34515/DATA.ERG-06001

Matsuoka, A., Teramoto, M., Nomura, R., Nosé, M., Fujimoto, A., Tanaka, Y., et al. (2018). The Arase (ERG) magnetic field investigation. *Earth Planets and Space*, *70*(1), 43.

Meredith, N. P., Horne, R. B., Glauert, S. A., & Anderson, R. R. (2007). Slot region electron loss timescales due to plasmaspheric hiss and lightning-generated whistlers. *Journal of Geophysical Research*, *112*, A04207. https://doi.org/10.1029/2007JA012413

Meredith, N. P., Horne, R. B., Thorne, R. M., & Anderson, R. R. (2003). Favored regions for chorus-driven electron acceleration to relativistic energies in the earth's outer radiation belt. *Geophysical Research Letters*, *30*(16), 1871. https://doi.org/10.1029/2003GL017698

Miyashita, Y., Shinohara, I., Fujimoto, M., Hasegawa, H., Hosokawa, K., Takada, T., & Hori, T. (2011). A powerful tool for browsing quick-look data in solar-terrestrial physics: "Conjunction event finder". *Earth Planets and Space*, *63*(1), e1.

Miyoshi, Y., Hori, T., Shoji, M., Teramoto, M., Chang, T.-F., Segawa, T., et al. (2018). The ERG science center. *Earth Planets and Space*, *70*(1), 1–11.

Miyoshi, Y., Morioka, A., Misawa, H., Obara, T., Nagai, T., & Kasahara, Y. (2003). Rebuilding process of the outer radiation belt during the 3 November 1993 magnetic storm: NOAA and Exos-D observations. *Journal of Geophysical Research*, *108*(A1), 1004. https://doi.org/10.1029/2001JA007542

Miyoshi, Y., Shinohara, I., & Jun, C.-W. (2018). The level-2 orbit data of exploration of energization and radiation in geospace (ERG) Arase satellite. Nagoya, Japan: ERG Science Center, Institute for Space-Earth Environmental Research, Nagoya University. https://doi.org/10.34515/DATA.ERG-12000

Miyoshi, Y., Shinohara, I., Takashima, T., Asamura, K., Higashio, N., Mitani, T., et al. (2018). Geospace exploration project ERG. *Earth Planets and Space*, *70*(1), 101.

Němec, F., Bezděková, B., Manninen, J., Parrot, M., Santolík, O., Hayosh, M., & Turunen, T. (2016). Conjugate observations of a remarkable quasiperiodic event by the low-altitude demeter spacecraft and ground-based instruments. *Journal of Geophysical Research: Space Physics*, *121*, 8790–8803. https://doi.org/10.1002/2016JA022968

Němec, F., Hospodarsky, G., Bezděková, B., Demekhov, A., Pasmanik, D., Santolík, O., & Hartley, D. (2018). Quasiperiodic whistler mode emissions observed by the van Allen probes spacecraft. *Journal of Geophysical Research: Space Physics*, *123*, 8969–8982. https://doi.org/10.1029/2018JA026058

Němec, F., Hospodarsky, G., Pickett, J. S., Santolík, O., Kurth, W. S., & Kletzing, C. (2016). Conjugate observations of quasiperiodic emissions by the cluster, van Allen probes, and Themis spacecraft. *Journal of Geophysical Research: Space Physics*, *121*, 7647–7663. https://doi.org/10.1002/2016JA022774

Ozaki, M., Yagitani, S., Nagano, I., Hata, Y., Yamagishi, H., Sato, N., & Kadokura, A. (2008). Localization of VLF ionospheric exit point by comparison of multipoint ground-based observation with full-wave analysis. *Polar Science*, *2*(4), 237–249.

Ozaki, M., Yagitani, S., Nagano, I., Yamagishi, H., Sato, N., & Kadokura, A. (2009). Estimation of enhanced electron density in the lower ionosphere using correlation between natural VLF waves and CNA. *Antarctic Record*, *53*(2), 123–135.

Santolik, O. (2008). New results of investigations of whistler-mode chorus emissions. *Nonlinear Processes in Geophysics*, *15*(4), 621–630.

Santolík, O., Macúšová, E., Kolmašová, I., Cornilleau-Wehrlin, N., & de Conchy, Y. (2014). Propagation of lower-band whistler-mode waves in the outer van Allen belt: Systematic analysis of 11 years of multi-component data from the cluster spacecraft. *Geophysical Research Letters*, *41*, 2729–2737. https://doi.org/10.1002/2014GL059815

Santolík, O., Parrot, M., & Lefeuvre, F. (2003). Singular value decomposition methods for wave propagation analysis. *Radio Science*, *38*(1), 1010. https://doi.org/10.1029/2000RS002523

Sato, N., Hayashi, K., Kokubun, S., Oguti, T., & Fukunishi, H. (1974). Relationships between quasi-periodic VLF emission and geomagnetic pulsation. *Journal of Atmospheric and Terrestrial Physics*, *36*(9), 1515–1526.

Sazhin, S., & Hayakawa, M. (1992). Magnetospheric chorus emissions: A review. *Planetary and Space Science*, *40*(5), 681–697.

Sazhin, S., & Hayakawa, M. (1994). Periodic and quasiperiodic VLF emissions. *Journal of Atmospheric and Terrestrial Physics*, *56*(6), 735–753.

Shiokawa, K., Yokoyama, Y., Ieda, A., Miyoshi, Y., Nomura, R., Lee, S., & Connors, M. (2014). Ground-based ELF/VLF chorus observations at subauroral latitudes VLF-chain campaign. *Journal of Geophysical Research: Space Physics*, *119*, 7363–7379. https://doi.org/10.1002/2014JA020161

Smith, A. J., Engebretson, M. J., Klatt, E. M., Inan, U. S., Arnoldy, R. L., & Fukunishi, H. (1998). Periodic and quasiperiodic ELF/VLF emissions observed by an array of Antarctic stations. *Journal of Geophysical Research*, *103*(A10), 23611–23622.

Smith, R., Helliwell, R., & Yabroff, I. (1960). A theory of trapping of whistlers in field-aligned columns of enhanced ionization. *Journal of Geophysical Research*, *65*(3), 815–823.

Thorne, R. M. (2010). Radiation belt dynamics: The importance of wave-particle interactions. *Geophysical Research Letters*, *37*, L22107. https://doi.org/10.1029/2010GL044990

Thorne, R. M., Smith, E. J., Burton, R. K., & Holzer, R. E. (1973). Plasmaspheric hiss. *Journal of Geophysical Research*, *78*(10), 1581–1596.

Titova, E., Kozelov, B., Demekhov, A., Manninen, J., Santolik, O., Kletzing, C., & Reeves, G. (2015). Identification of the source of quasiperiodic VLF emissions using ground-based and van Allen probes satellite observations. *Geophysical Research Letters*, *42*, 6137–6145. https://doi.org/10.1002/2015GL064911

Tsyganenko, N., & Sitnov, M. (2005). Modeling the dynamics of the inner magnetosphere during strong geomagnetic storms. *Journal of Geophysical Research*, *110*, A03208. https://doi.org/10.1029/2004JA010798

Tsyganenko, N. A., & Stern, D. P. (1996). Modeling the global magnetic field of the large-scale Birkeland current systems. *Journal of Geophysical Research*, *101*(A12), 27187–27198.